JOURNAL OF GEOPHYSICAL RESEARCH, VOL. 113, D06306, doi:10.1029/2007JD008706, 2008

Aerosol and trace-gas measurements in the Darwin area during the wet season

G. Allen,[1] G. Vaughan,[1] K. N. Bower,[1] P. I. Williams,[1] J. Crosier,[1] M. Flynn,[1] P. Connolly,[1] J. F. Hamilton,[2] J. D. Lee,[2] J. E. Saxton,[2] N. M. Watson,[2] M. Gallagher,[1] H. Coe,[1] J. Allan,[1] T. W. Choularton,[1] and A. C. Lewis[2]

Received 27 March 2007; revised 9 July 2007; accepted 16 November 2007; published 29 March 2008.

[1] The composition of the planetary boundary layer in regions of deep tropical convection has a profound impact on the Tropical Tropopause Layer (TTL). The Aerosol and Chemical Transport in tropIcal conVEction (ACTIVE) aircraft campaign was conducted from November 2005 to February 2006 from Darwin, Australia, to characterize the influence of both monsoonal and localized land-based deep convection on the composition of the TTL. This paper summarizes the composition of the potential inflow to such convection in terms of aerosol particle size and composition, carbon monoxide, and ozone, as measured in the lowest 4 km of the atmosphere by the NERC Dornier-228 aircraft during 28 flights in different meteorological regimes over the course of ACTIVE. Six contrasting periods are identified in the boundary layer background as a result of the prevailing meteorology and sources of pollution. The campaign began with a relatively polluted and variable biomass burning season in November, followed by a transition to the monsoon season through December with much less burning. A clean maritime flow dominated the wet-active, and dry-inactive, monsoon period in January; it was followed by a monsoon break period in February, with a return to continental flow and a more premonsoon background state. Deep convective systems, capable of transporting boundary layer air to the TTL, were observed daily outside of the monsoon periods. The chemical composition of submicron aerosols in the premonsoon periods was dominated by a mix of fresh and aged organic material with significant black carbon, well-correlated with carbon monoxide indicating a common burning source, while marine aerosol during the monsoon changed markedly between the wet and dry phases. High concentrations of coarse-mode aerosols were also observed in the monsoon: the clean, marine air masses and high surface winds imply that sea salt may be the dominant aerosol type under these conditions. The climatology presented here will provide a valuable data set for model simulation of chemical and aerosol transport by deep convection in the Darwin region.

Citation: Allen, G., et al. (2008), Aerosol and trace-gas measurements in the Darwin area during the wet season, *J. Geophys. Res.*, *113*, D06306, doi:10.1029/2007JD008706.

1. Introduction

[2] Tropical convection is a crucial issue for climate science for many reasons: Tropical cloud composition (e.g., ice water, liquid water, black carbon) and cloud-top height have profound implications for the Earth's radiative budget; and fast transport (a few hours) of surface boundary layer trace gases and particles to the upper troposphere affect its composition and chemistry [*Dessler*, 2002]. The Tropical Tropopause Layer (TTL) is the subject of much ongoing study to reduce uncertainty in climate change predictions and the nature of stratosphere-troposphere exchange [*Stohl et al.*, 2003] and consequent impacts on stratospheric ozone [*Esler et al.*, 2001]. Furthermore, aerosol particles lifted from the surface have indirect effects influencing precipitation and radiation fluxes [*Lohmann and Feichter*, 2005; *McFiggans et al.*, 2006]. For example, the convective uplift of black carbon aerosol generated by frequent biomass burning in the tropics can perturb the radiative equilibrium of the atmosphere; with both the sign and magnitude of the resultant net forcing noted to be highly uncertain and highly dependent on the overall particle composition and position in the atmosphere [*Intergovernmental Panel on Climate Change*, 2001]. Therefore, a better knowledge of tropical boundary layer composition is implicit in a better understanding of tropical convection and better characterization of the TTL environment.

[3] The UK Natural Environment Research Council (NERC)-funded ACTIVE campaign described by *Vaughan et al.* [2008] was conceived as a comprehensive research

[1]Centre for Atmospheric Science, University of Manchester, Manchester, UK.
[2]Department of Chemistry, University of York, Heslington, UK.

0148-0227/08/2007JD008706$09.00

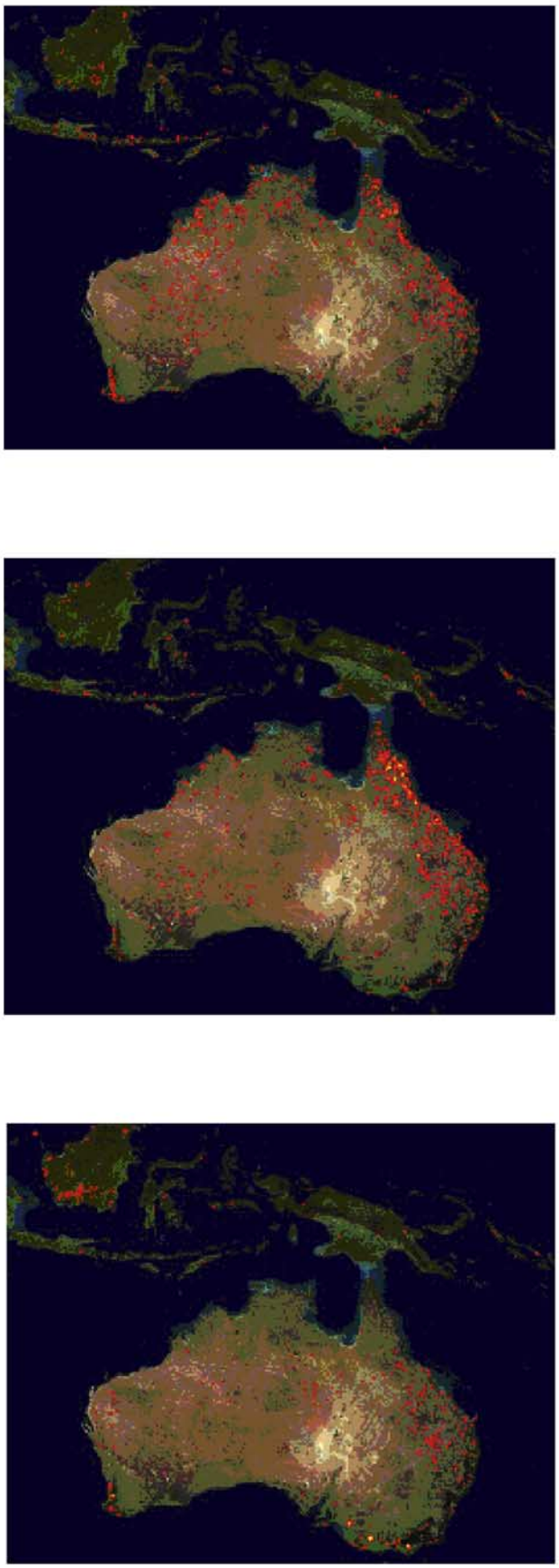

program of field measurements and modeling work to address these key scientific questions. This campaign took place during the 2005/2006 wet season (November–February) in Darwin, Australia (12.47°S, 130.85°E), and employed two aircraft: the Dornier 228-101 operated by the NERC Airborne Research and Survey Facility, and the Grob G520T Egrett aircraft operated by Airborne Research Australia. Instrumentation on the Dornier measured the aerosol and chemical background of the boundary layer and lower free troposphere between 100 and 4000 m (see section 2), while the Egrett measured cirrus cloud microphysics and outflow from deep convection up to an operational ceiling of 15 km. Furthermore, a total of 35 ozonesondes were launched throughout the campaign from Darwin Airport to provide simultaneous profiles of horizontal winds, pressure, temperature, relative humidity and ozone concentration.

[4] ACTIVE was one component of a comprehensive field experiment conducted during 2005/2006 to study TTL composition and clouds in the Darwin region, the other two being the SCOUT-O3 campaign between 15 November 2005 and 8 December 2005 also described by *Vaughan et al.* [2008] and the Tropical Warm Pool International Cloud Experiment (TWP-ICE) conducted between 21 January 2006 and 14 February 2006. Further aircraft measurements in the TTL, and meteorological measurements in the boundary layer, were conducted by these projects, while radiosondes were launched every six hours as part of TWP-ICE from a network of locations around Darwin during TWP-ICE. Together, these synergistic campaigns generated an unprecedented data set from which to study tropical deep convection.

[5] The Darwin region offers a unique location from which to conduct studies of tropical convection, owing to its proximity to the tropical warm pool around Indonesia and to the Tiwi Islands situated 150 km to the north. So-called Hector thunderstorms occur almost daily over the Tiwis during the premonsoon and monsoon-break periods between November and February as a result of the strong convergence of warm, moist sea and land breezes [*Crook*, 2000]. In addition, the annual monsoon flow initiates large-scale uplift in the area [*Manton and McBride*, 1992]. In order to understand the impact on the TTL of these convective influences it is necessary to first understand the composition of the boundary layer and hence the inflow to local convective storms in order to relate observations of the high-altitude outflow with those made in the inflow region. This paper derives representative summaries of gas phase and aerosol size and composition data measured by the NERC Dornier aircraft for various meteorological regimes encountered during ACTIVE.

[6] The main sources of aerosol expected around the Darwin area are from biomass burning, the local maritime environment and possible dry soil disturbance, potentially lofting mineral dust. Biomass burning in the northern Australian savanna occurs very frequently throughout the

Figure 1. MODIS-derived fire maps of the Australasian region integrated between: (top) 17 and 30 November 2005; (middle) 7 and 12 December 2005, and (bottom) 21 and 30 January 2005. Red areas show active fires. Images courtesy of MODIS Rapid Response Project at NASA/GSFC.

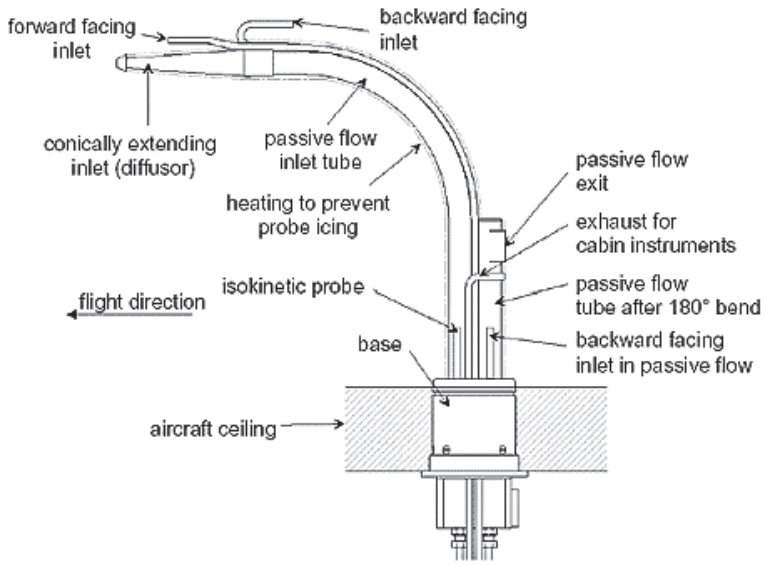

Figure 2. Dornier aerodynamic inlet configuration (Figure courtesy of Andreas Petzold, Deutsche Zentrum für Luft und Raumfahrt).

dry season (June to November) with average annual fuel loadings of up to 9.2 t ha^{-1} as estimated by *Russell-Smith et al.* [2003] for the nearby Arnhem Land region during 1999. Fire maps derived using the method described *Giglio et al.* [2003] and *Davies et al.* [2004] from the Moderate Resolution Imaging Spectroradiometer (MODIS) instrument on NASA's TERRA satellite, are shown in Figure 1, which show the prevalence of biomass fires across the Northern Territory in November 2005 (Figure 1, top); and in contrast, an absence of such fires in the region by December (Figure 1, middle) and a continued absence into late January (Figure 1, bottom). Fires in the Queensland region (over 1500 km to the east) are evident at all times throughout the campaign, with greater intensity during November/December than in January/February.

[7] Burning emissions in the Northern Territory were extensively studied by the Biomass Burning and Lightning Experiment (BIBLE) campaign described by *Kondo et al.* [2002], which concentrated predominantly on gas phase emissions and the wider Asian and Indonesian environment, with some observations of aerosols and black carbon [*Liley et al.*, 2002]. The bulk of such burning early in the dry season is initiated by land managers and is relatively low in intensity to remove denser undergrowth that has built up over the preceding wet season. Toward the end of the dry season, fires become more intense as drier fuel sources are consumed. This is particularly the case in Arnhem Land to the east of Darwin, where grassy fuel dries out later in the year compared with the western regions, and is thus prone to fires being started owing to lightning or accident. On any given day, the number and location of fires can vary greatly with background smoke levels between June and September reported to change markedly [*Carr et al.*, 2005] with a tendency toward increasing smoke accumulation and larger particle sizes throughout the period. Hence we expect such burning to influence the local boundary layer for the first weeks of the ACTIVE campaign, when prevailing surface winds were easterly (see section 4).

[8] In contrast to the premonsoon, maritime air is expected to dominate during active monsoon episodes, albeit with the potential for mixing of transported continental air masses. To our knowledge, no previous studies of the aerosol background in Northern Australia during the wet season have taken place, a need highlighted by *Heintzenberg et al.* [2000].

[9] The boundary layer CO burden near Darwin is expected to show a general relationship to the aerosol burden, reflecting the nature of common pyrogenic sources. However, episodic influences of long-range transport of pollutants to northern Australia from sources such as South America and South Africa in austral spring have been reported for CO as retrieved from satellite observations [*Gloudemans et al.*, 2006]. Hence we see that the Darwin boundary layer environment is influenced not only by local sources but also by the governing meteorology and potentially more distant sources of pollution. This paper aims to illustrate this contrast throughout typical meteorological regimes encountered between November and February in the region.

2. Dornier-228: Mission and Instrumentation

2.1. Aerosol and Gas Inlet

[10] The Dornier-228 is a light twin-engine aircraft with an interior cabin modified to harbor a scientific payload. Ambient air was sampled through a purpose-built stainless steel, forward-facing, passive, isokinetic inlet positioned over the centre of the cockpit (see Figure 2). The inlet was manufactured by Deutsche Zentrum für Luft und Raumfahrt (DLR) and based on the aerosol inlet on the DLR Falcon aircraft. Transmission for this inlet is calculated to be 95% at 0.9 μm, 75% at 1.6 μm and 50% at $\sim$2.5 μm particle diameter. For further technical information relating to this inlet see *Fiebig* [2001] and *Petzold et al.* [2002]. From the main aerosol manifold, two isokinetic subsamples were taken: one branch fed the aerosol spectrometers and a particle

Table 1. Aerosol Instruments Onboard the Dornier Aircraft With Measured Size Ranges Given Where Appropriate[a]

Instrument	Size Range (Diameter)	Technique	Reference/Company
UHSAS	0.055–0.8 μm	optical scattering	Droplet Measurement Technologies Inc
Grimm 1.108	0.3–25 μm	optical counter	Grimm Technologies Inc
ASP	0.21–4.5 μm	optical scattering	Droplet Measurement Technologies Inc
FSSP	0.5–32 μm	optical scattering	*Baumgardner et al.* [1985]
TSI-1301D	>10 nm	condensational growth	*Agarwal and Sem* [1980]
PSAP	-	integration plate	Radiance Research Inc
AMS	0.04–0.7 μm	70 eV quadrupole mass spectrometry	*Jayne et al.* [2000]
Filters	-	particle deposition	

[a]See text for a further description of each instrument.

soot absorption photometer (detailed in section 2.3) on the port side of the aircraft, with the other feeding an aerosol mass spectrometer, a condensation particle counter and deposition filters on the starboard side. Each branch was further split isokinetically to feed the individual instruments. The gas phase instruments were fed from a rearward facing inlet on the main manifold (see Figure 2), while the exhaust from all instruments vented to the aft of the cabin. Transmission and diffusive losses after the inlet were calculated using aerodynamic theory outlined by *Baron and Willeke* [1993] and were found to be negligible across the size range of particles discussed in this work up to the 50% transmission cut-off diameter of the main inlet (2.5 μm). Hence, transmission losses were dominated by the main inlet for supermicron particles.

2.2. Thermodynamic Instrumentation

[11] Temperature, pressure, relative humidity and wind vectors, as well as GPS position and aircraft orientation, were sampled at 20 Hz and recorded at 1 Hz by a Aircraft Integrated Meteorological Measuring System (AIMMS) 20 Hz probe manufactured by Aventech Research Inc. and described further by *Beswick et al.* [2007]. The probe was positioned on a starboard wing-mounted pod. Typical air speed and aircraft pitch angle on science runs were 75 m s^{-1} and +4.5°, respectively.

2.3. Aerosol Instrumentation

2.3.1. Number and Size

[12] Aerosol particle number size distributions from 55 nm to 32 μm diameter were measured using a range of optical probes (see Table 1). Herein, the terms fine mode and coarse mode aerosol refer to the submicron and supermicron aerosol population fraction respectively. Optical scattering instruments included: (1) a Droplet Measurement Technologies (DMT, Boulder, CO, USA) ultra high sensitivity aerosol spectrometer (UHSAS), measuring dry fine mode aerosol size spectra at 1 Hz (averaged to 1/6 Hz) with a fine size resolution (7.5 nm bins) in the range 55 nm to 800 nm; (2) a prototype DMT aerosol spectrometer probe (ASP), measuring dry aerosol with a resolution between 0.1 and 0.2 μm in the range 0.21 to 4.5 μm; (3) a Grimm Aerosol Technik (GmbH) 1.108 optical particle counter (Ainring, Germany), measuring dry size ranges with a resolution between 0.03 and 0.5 μm in the range 0.3 to 25 μm; and (4) for the coarse aerosol component, a wing-mounted forward scattering spectrometer probe (FSSP-100), described further by *Baumgardner et al.* [1985], measuring ambient particle number size distributions with resolution 0.8 μm from 0.5 to 32 μm. In addition, a TSI-3010D (TSI Inc., Shoreview, MN, USA) condensation particle counter (CPC) measured the total particle number concentration greater than ~10 nm. However, absolute number concentrations for sizes greater than 2 μm measured by the ASP and Grimm instruments are not considered here owing to inlet transmission limitations (50% transmission at 2.5 μm).

2.3.2. Black Carbon

[13] A Radiance Research Inc particle soot absorption photometer (PSAP) measured black carbon content. For this study, the soot absorption cross section (σ_{ae} = 8.2 m^2g^{-1}) used by *Liley et al.* [2002] for the geographically similar BIBLE campaign is assumed. To account for high measurement noise, 0.2 Hz PSAP data were smoothed over a five-minute period. In stable operating conditions the PSAP sensitivity to changes in filter absorption gives a precision of 10^{-6} m^{-1}, or roughly 0.02 μg m^{-3} of soot for five-minute integration.

2.3.3. Composition

[14] A Quadrupole Aerodyne Aerosol Mass Spectrometer (Q-AMS) system [*Jayne et al.*, 2000], which sampled air through the main manifold, was used to determine the mass loading of the nonrefractory, non-sea-salt chemical component of submicron aerosol with a high time resolution (30 s). This instrument employs thermal desorption, 70 eV electron ionization, and a quadrupole mass spectrometer. Data were processed and quality assured using the procedures described by *Jimenez et al.* [2003] and *Allan et al.* [2003, 2004a] and employed in conjunction with the pressure-dependent calibrations and corrections described by *Crosier et al.* [2006] needed for aircraft operation. Mass concentrations are reported from the Q-AMS (see section 5) for the total nitrate, organic, sulphate and ammonium component masses in the aerosol. Component mass size distributions could not be derived here with sufficient confidence (reasonable signal to noise) owing to the relatively clean environment sampled throughout the majority of ACTIVE flights.

2.4. Gas Phase Instrumentation

[15] Gas phase instruments onboard the Dornier are summarized in Table 2 and consisted of the following.

2.4.1. Carbon Monoxide

[16] Measurement of CO was performed in-flight using a fast response fluorescence instrument; the AL5002 fast carbon monoxide (CO) monitor (Aero-Laser GmbH, Garmisch-Partenkirchen, Germany), fitted with a Nafion dryer to remove water vapor. With an integration time of ten seconds, the detection limit was better than 2.0 ppbv. The linearity

Table 2. Gas Phase Instrumentation and Measurement Technique on the Dornier Aircraft

Instrument	Technique	Gases	Reference/Company
Aerolaser AL5002	fluorescence	CO	Aerolaser Inc
2B Technologies 202 ozone analyzer	UV absorption	O_3	2B Technologies
Automatic tube sampler	absorbent trapping and GC-MS	C5-C10 aliphatics, aromatics monoterpenes, OVOCs	University of York
Miniature GC	gas chromatography	halocarbons (Cl, Br, I)	*Robinson et al.* [2000]

range of the instrument was 0–100 ppmv; well beyond the typical concentrations encountered during ACTIVE. Calibration of the instrument was performed in-flight at various flight levels to allow for the potential effect of ambient pressure changes, using a secondary gas standard containing 73 ppbv ± 5% CO in synthetic air. An additional standard (200 ppbv) was used throughout the campaign to validate the in-flight standard. Data were recorded at one-second intervals.

2.4.2. Ozone

[17] Ozone was measured in-flight using a UV absorption detector (2B Technologies). Calibration was carried out prior to deployment using gas phase titration of NO. Data were collected at ten second intervals with an overall uncertainty of 5% (±2 ppbv). Concentration resolution is approximately 1 ppbv.

2.4.3. Volatile Organic Compounds (VOCs)

[18] Additional measurements of a range of VOCs were also obtained onboard the Dornier using adsorbent tube samplers and postflight thermal desorption coupled to comprehensive two-dimensional gas chromatography with time-of-flight mass spectrometry (see *Saxton et al.* [2007] for further details). Calibration was achieved using a 74 component gas standard at 0.1–2 ppbv levels (Apel Reimer) and uncertainties on single measurements of all VOCs derived by this method are typically around 20% of the determined concentration. Species measured include: isoprene, α-pinene, ethyl benzene, m+p xylene, o-xylene, nonane, isopropyl benzene, 3-ethyl toluene, 1, 3, 5-trimethyl benzene, 1, 2, 4- trimethyl benzene, and 1, 2, 3- trimethyl propyl benzene. Isoprene and α-pinene are not discussed further here owing to their very low atmospheric lifetimes (of the order 1 hour) and high spatial variability (e.g., land/sea contrast) making any overall analysis of their concentration meaningless.

2.5. Flight Operations

[19] A total of eleven Dornier science flights and one test flight were carried out in the first phase of the campaign between 13 November and 5 December 2005, of which eight were circumnavigations of the Tiwi Islands to the north of Darwin during the development of Hector-type convection, and three were survey flights of the wider Darwin region (See Table 3 for a summary). A further sixteen flights were conducted in the second phase between 19 January and 14 February 2006, of which three were survey flights of the wider region, four studied the inflow to monsoon convection and a further four measured inflow to Hector systems.

[20] Other flights in the second phase included two survey flights to study a monsoon trough inland between Darwin and Alice Springs and a further two flights to sample potentially contrasting air masses toward Indonesia. These four flights are not considered further here as they are not relevant to the climatological background of convective inflow near Darwin. An additional flight was performed to compare simultaneous measurements alongside the Egrett aircraft (see section 3) for the purposes of instrument intercomparison.

3. Data Quality

3.1. Meteorological Data Quality

[21] Meteorological measurements made by the AIMMS-20 probe were compared with radiosonde profiles launched from Darwin Airport and additionally with the six-hourly TWP-ICE radiosonde network in January and February. Comparisons of the AIMMS temperature measurements with closely coincident radiosondes gave random differences of ±1°C. Owing to horizontal variability in temperature these differences are not considered significant and no corrections were applied to the data. The instrument manufacturers claim an accuracy of 0.3°C for AIMMS temperature.

Table 3. A Summary of Dornier-228 Missions Throughout ACTIVE

Date	Flight Label[a]	Primary Mission
8 Nov 2005	TD01	instrument test
13 Nov 2005	TD02	test/Tiwi survey
15 Nov 2005	AD03	Tiwi survey
16 Nov 2005	AD04	Tiwi survey[b]
19 Nov 2005	SD05	Tiwi Survey[b]
23 Nov 2005	SD06	inland survey
24 Nov 2005	SD07	inland survey
28 Nov 2005	AD08	Tiwi survey
30 Nov 2005	AD09	Tiwi survey[b]
1 Dec 2005	AD10	Tiwi survey
4 Dec 2005	AD11	Tiwi survey
5 Dec 2005	AD12	inland survey
19 Jan 2006	TD13	test/Tiwi survey
20 Jan 2006	AD14	monsoon inflow (Tiwis)
22 Jan 2006	AD15	monsoon inflow (Inland)[c]
25 Jan 2006	AD16	Tiwi survey[c]
26 Jan 2006	SD17	inland survey
27 Jan 2006	SD18	inland survey[c]
30 Jan 2006	SD19	Northern Hemisphere plume
1 Feb 2006	SD20	survey to Alice Springs
2 Feb 2006	SD21	survey (return to Darwin)
3 Feb 2006	SD22	Northern Hemisphere plume
6 Feb 2006	AD23	Tiwi survey[c]
8 Feb 2006	AD24	Tiwi survey[c]
9 Feb 2006	AD25	Tiwi survey
10 Feb 2006	AD26	Tiwi survey[c]
12 Feb 2006	AD27	inland survey
14 Feb 2006	AD28	instrument intercomparison

[a]First letter of flight label denotes mission type (T, test; A, convective inflow mission; S, wider area background survey), while the second letter signifies the Dornier aircraft.
[b]Coincident with SCOUT-O3 mission.
[c]Coincident with TWP-ICE mission.

Table 4. Periods of Meteorological Contrast During ACTIVE Flight Operations

Period	Prevailing Influence	Flights Within Period
13–19 Nov + 25–30 Nov	biomass burning	TD02–SD05 + AD08-AD09
20–24 Nov	mini-monsoon	SD06–SD07
30 Nov to 5 Dec	premonsoon	AD10–AD12
14–22 Jan	active monsoon	TD13–AD15
25–27 Jan	inactive monsoon	AD16–SD18
4–14 Feb	monsoon break	AD23–AD28

[22] Relative humidity (RH), static pressure and wind data recorded by the AIMMS probe were compared with the sonde data set and with Rotronic HygroClip SC05 temperature and humidity sensors in the AMS sample line. A direct quantitative comparison of AIMMS RH with sondes is limited by the very high natural horizontal variability; however, no systematic differences were noted in November and December and the AIMMS and Rotronic sensors agreed to within 10% (after correcting the latter for the temperature and pressure difference between the atmosphere and inlet line). In the second phase of the campaign, the AIMMS probe was noted to have developed a technical problem due to contamination, with frequently recorded unrealistic RH in excess of 120% and consistent differences of up to 60% between AIMMS and Rotronic sensors. Therefore, RH measurements (corrected for ambient pressure and temperature) recorded by the Rotronic sensor are used for all Dornier flights in the second phase of ACTIVE.

[23] General agreement in horizontal wind direction and wind speed was found between radiosondes and AIMMS, and AIMMS pressure was noted to be highly consistent (to within 1 mb) with sonde profiles of pressure at equivalent altitudes.

3.2. Aerosol Data Quality

[24] The multiplicity of aerosol spectrometer instruments with overlapping size ranges in ACTIVE allows good characterization of each instrument and better confidence in the accuracy of quantitative data. Median values of total aerosol number concentration for the Grimm, ASP and UHSAS, in their common size range of 0.3 to 0.8 μm, were calculated for each Dornier flight and compared.

[25] The average ratio of medians from each flight between the Grimm and ASP spectrometers was 1.71 ± 0.26 in the first phase of the campaign and 1.58 ± 0.20 in the second phase; therefore we conclude that these two instruments were reasonably consistent with each other throughout the whole campaign, in that neither instrument developed a significant drift in sensitivity. However, the UHSAS developed a technical fault after the end of the first phase of ACTIVE and its data are considered unreliable for the later period. The Grimm and ASP worked correctly throughout the campaign, so owing to its greater spectral size resolution, the fine mode aerosol number concentrations reported in this work are taken from the ASP instrument. Differences between the instruments in the first phase serve here as an indication of the inherent uncertainties in using optical probes; variations in particle shape and (complex) refractive index can result in ambiguities in the scattering properties of the aerosol under investigation [*Liu and Daum*, 2000].

[26] For the AMS, a collection efficiency of 0.5 was used, typical of the value obtained through comparisons with other instruments in the field [*Allan et al.*, 2004b; *Takegawa et al.*, 2005]. This was validated through a comparison between the integrated UHSAS total particulate volume and the summed AMS and PSAP particulate volume measurements, assuming a density of 1.77 g cm^{-3} for inorganic aerosol and 1.2 g cm^{-3} for organics, as derived by *Cross et al.* [2007]. Average ratios of UHSAS integrated volume to summed AMS and PSAP volumes were in the range 0.4 to 0.7.

3.3. Gas-Phase Data Quality

[27] Carbon monoxide and ozone measurements onboard the Dornier were compared with instrumentation on the Egrett aircraft during purpose-flown intercomparison flights where both flew in formation. One such flight was performed in each measurement phase. Carbon monoxide differed by 10 ppbv at most between the two aircraft's instruments so we take 10 ppbv as the uncertainty on CO data and note that the interseasonal variability measured during ACTIVE greatly exceeds this.

[28] A comparison for ozone in the first phase was not possible owing to a failure of the Egrett ozone instrument. A flight intercomparison in the second phase showed that the Dornier ozone instrument measured more than the Egrett's by ~7 ppbv. However, problems were noted with the Egrett instrument due to systematic differences in measured concentration between ascent and descent. Dornier ozone profiles were also compared with ozonesondes launched from Darwin Airport (where available). Although differences of up to 10 ppbv were observed on flights where measured spatial variability in ozone was high, with the Dornier tending to read less than the sondes on average, much of this is expected to be due to naturally high horizontal variability. On flights where little spatial variability was observed in the Dornier data, and the PBL ozonesonde profile varied smoothly with altitude, differences were much smaller (<2 ppbv).

4. Prevailing Meteorology

[29] Six contrasting periods are identified here for the purposes of deriving representative climatologies on the basis of contrasting meteorology and biomass burning influences. These periods and the science flights conducted in each period are summarized in Table 4. Data from all flights within each period are used to derive the summaries presented in section 5. The contrasting meteorology of each period is discussed in the remainder of this section.

4.1. Biomass Burning

[30] During the first phase of the ACTIVE campaign, typical premonsoon conditions prevailed at Darwin. For most of this period the lower level winds were dominated by easterly flow at 700 mb (the convective steering level) with wind speeds between 12 to 20 m s^{-1}. At the surface, local sea-breeze circulations generated a range of convective storms, from isolated island thunderstorms to squall line

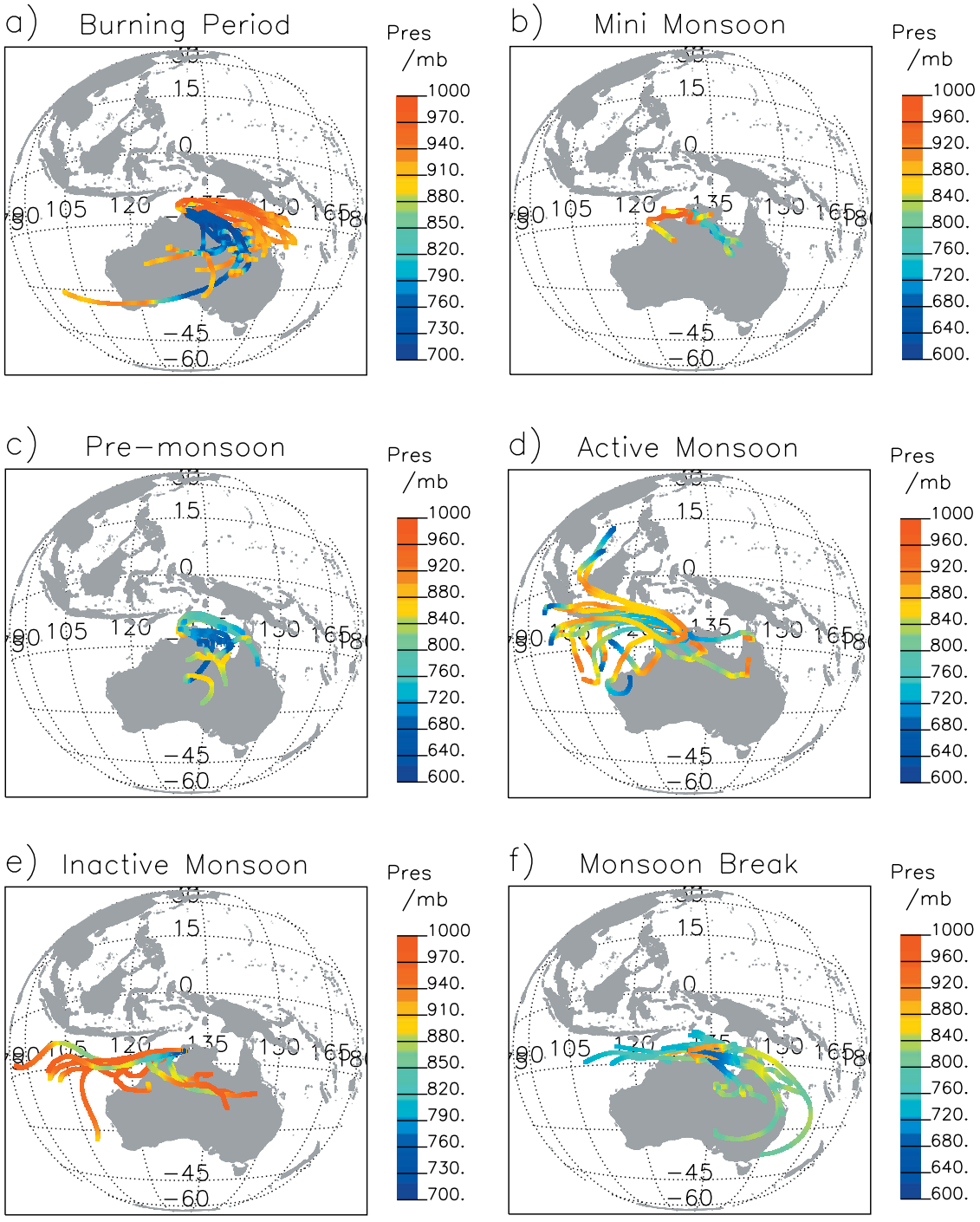

Figure 3. Five-day ECMWF back-trajectories initiated from Darwin (130.9°E, −12.41°S) at 700 mb and 900 mb at 0600 UTC (1530 local time) for every day within each time period indicated.

complexes ~100 km in scale. Such deep convective storm systems regularly achieved cloud top heights in excess of 18 km [*Vaughan et al.*, 2008] suggesting significant fast transport of boundary layer air to the TTL during this period. Back-trajectories of air sampled by the Dornier in the Darwin area generally tracked over Queensland and the Northern Territories over the previous five days (see Figure 3). Large-scale land clearance burning over Arnhem Land to the east of Darwin is evident from MODIS fire maps during this period (see Figure 1) with resulting plumes mixing into the easterly surface flow arriving at Darwin throughout this period. On occasion, fresh plumes from localized active burning on the Tiwi Islands were also sampled by the Dornier.

4.2. Mini Monsoon

[31] An exception to this general pattern occurred between 20 and 22 November, during which a 'mini monsoon'

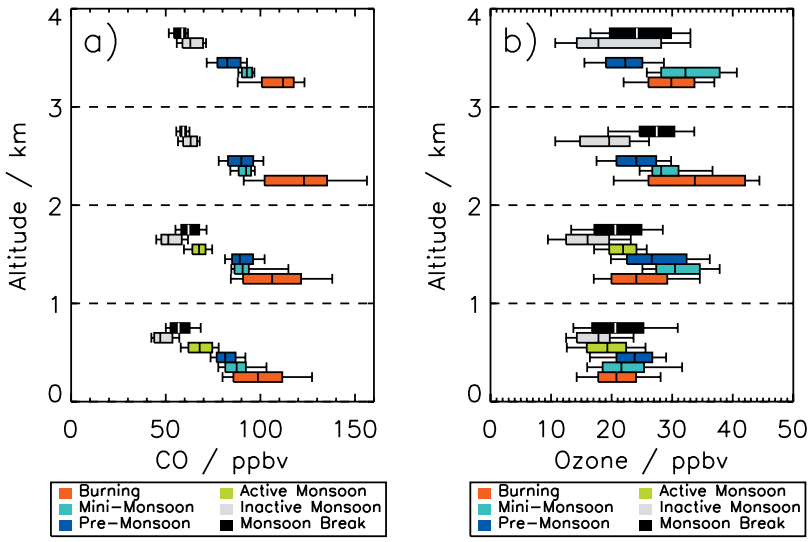

Figure 4. Average boundary layer profiles of (a) carbon monoxide and (b) ozone, color-coded by time period as indicated. The box center denotes the median concentration; box edges denote the upper and lower quartiles; and extremities denote the 10th and 90th percentile concentrations. Note that no measurements were made above 2 km in the active monsoon period.

was experienced, so named because of a deep westerly flow from 700 mb to 200 mb coincident with widespread oceanic convection. This period was not a true monsoon in the meteorological sense, but the resultant oceanic convection and deep maritime flow greatly resembled monsoon conditions. This reversal in the prevailing winds was associated with an unusually strong northward undulation of the subtropical jet stream and a significant westerly momentum injection to the free troposphere associated with a breaking Rossby wave. Back trajectories initiated at 900 mb and 700 mb during this time show easterly and westerly origins respectively, suggesting that clean maritime air at low levels would have been overlaid with relatively polluted air arriving from the burning regions to the east. Deep convection initiated by sea-breeze circulations was absent during these few days owing to the strong wind shear associated with the passage of the Rossby wave, with the observed maritime convection reaching cloud top heights much less than 10 km.

4.3. Premonsoon

[32] Following a return to a prevailing easterly flow after the passage of the Rossby wave, back trajectories show a return to inland origins to the east and south of Darwin. However, MODIS fire maps (Figure 1) show that the number of biomass burning sites during this period were greatly reduced. Therefore, although the general meteorology was broadly similar to the biomass burning period discussed earlier, we can expect air masses sampled during this period to be much less influenced by local biomass burning sources. Similar sea-breeze circulations and isolated deep convective systems were observed daily during this period with the potential for significant fast transport to the TTL.

4.4. Active Monsoon

[33] Prior to the start of flight operations in the second phase of ACTIVE, a monsoon trough formed to the south of Darwin with a northwesterly monsoon flow from the surface to 300 mb developing by 14 January 2006. Back trajectories from Darwin during this period show a long-range westerly maritime origin for at least 5 days prior to sampling. Large-scale maritime convection was prevalent during this time with cloud top heights reaching up to the tropopause. This 'active monsoon' period persisted until 22 January 2006, when a monsoon low formed just to the north of Darwin and moved southward to the central Northern Territory.

4.5. Inactive Monsoon

[34] The inland monsoon low dominated the meteorology in the Darwin area until 3 February 2006, bringing a stable westerly airstream in the lower troposphere across the Darwin area which suppressed deep convection, with storms generally reaching no higher than 10 km. We refer to this period as the inactive monsoon.

4.6. Monsoon Break

[35] After 3 February, the monsoon low disappeared, and easterly flow gradually developed, initially at 700 mb but eventually leading to a deep easterly airflow as in the pre-monsoon period. Isolated deep convection became prevalent, initially as Hector storms over the Tiwi Islands, then eventually extending to the mainland giving similar conditions to the premonsoon. Convection also became more organized: single-cell Hector storms were observed on 6 February, intensifying to become multicellular from 9 February until the end of the campaign.

5. Results

5.1. Carbon Monoxide and Ozone

[36] Vertical profiles of median carbon monoxide (CO) and ozone concentration for each time period are plotted in Figure 4 together with upper and lower quartiles and 10th and 90th percentile whiskers. Data were averaged across

Table 5. Concentration Statistics for Carbon Monoxide and Ozone Within Each Meteorological Period Averaged for All Altitudes Greater Than 100 m[a]

	CO, ppbv							Ozone, ppbv						
Period	Mean	Standard Deviation	Median	10%	25%	75%	90%	Mean	Standard Deviation	Med	10%	25%	75%	90%
Biomass burning	112.3	20.7	102.4	80.8	88.6	116.4	136.4	25.3	3.6	24.2	16.3	20.0	29.7	35.5
Mini-monsoon	98.1	7.9	89.0	79.6	84.5	93.3	98.0	26.3	2.8	25.5	17.3	20.7	31.0	36.4
Premonsoon	88.9	4.1	86.4	75.8	80.5	92.3	96.7	25.1	2.7	24.7	18.0	21.2	28.8	33.3
Active monsoon	69.2	3.3	67.9	58.0	62.4	74.2	77.7	20.0	3.1	19.8	13.0	16.4	23.0	25.8
Inactive monsoon	52.3	8.5	51.5	43.2	45.5	57.9	62.8	17.5	3.1	17.8	10.7	14.0	20.2	24.6
Monsoon break	59.4	2.6	58.5	50.7	54.0	64.2	69.5	21.9	3.2	21.3	13.8	17.1	26.3	31.2

[a]Concentrations are quoted in parts per billion by volume.

those flights within each period in Table 4 within three vertical layers between 0 and 3 km with 1 km resolution and an additional box for altitudes greater than 3 km (note that the maximum altitude flown by the Dornier in the campaign was 4.1 km). To ensure that data used here are not contaminated by sources associated with airstrips (e.g., other aircraft, generators), all data below 100 m during take-off and landing have been discarded. Furthermore, very short-lived high concentrations (data spikes) have been removed; these probably occurred when engine exhaust was sampled owing to turbulent flow in steep ascending turns. More complete statistics averaged over all altitudes for each period are summarized in Table 5.

[37] Carbon monoxide is a useful, relatively long-lived (~2 months in the troposphere) tracer of many land-based pollution sources [*Staudt et al.*, 2001]. In the southern hemisphere the lack of strong anthropogenic fossil fuel sources makes CO a predominant marker of both fresh and aged biomass burning plumes and is typically well-correlated with aerosol number concentration [e.g., *Edwards et al.*, 2006]. In conjunction with ozone concentration and aerosol composition such as that afforded here by the AMS, CO can also be used to differentiate source type and age of polluted air masses. Carbon monoxide is discussed here in this context as a tracer of air mass origin and an indicator of background pollution levels.

[38] Figure 4 shows a clear evolution in background CO. In the biomass burning season, we see not only the highest levels of CO (~102 ppbv), but also the largest variability with a distribution extending to values in excess of 150 ppbv. The interquartile range is small relative to the difference between the 75th and 90th percentiles, reflecting a small number of very high CO events, which are associated with short flight legs targeted at sampling visually polluted layers (smoke) in fresh fire plumes. In the mini-monsoon period, there is a little less CO (~90 ppbv) in the background atmosphere and variability is reduced. This is consistent with the introduction of cleaner maritime air in the westerly flow during this period, coupled with a reduction in the intensity of fires inland due to increased rainfall. However, the general background is still high in CO (relative to succeeding periods) and therefore better characterized in terms of burning influences. The premonsoon is cleaner still with an overall median concentration of 86 ppbv and much less variability than the burning-dominated period. This premonsoon period represents similar meteorology to the polluted burning season, with the major difference being the absence of inland fires.

[39] Throughout both the active and inactive monsoon periods, CO continues to fall and shows very low variability within each period as cleaner maritime air was drawn into the Darwin area from the west. In the cleanest period (51 ppbv in the inactive monsoon), ten-day back-trajectories indicate advection from the remote Southern Ocean associated with circulation around the dominant inland depression throughout this period. The monsoon break shows a slight increase in CO (~58 ppbv), expected to be due to build up from local sources and longer-range transport of continental air shown by back-trajectory analysis.

[40] Ozone, unlike CO, is a relatively short-lived (~1 week) species, with production and loss rates being highly dependent on the local chemical environment (e.g., NO_x). Ozone was very low (around 20 ppbv for much of the campaign) in comparison to northern hemispheric background concentrations (e.g., 64 ppbv in the central US reported by *Lefohn et al.* [2001]) and showed little change between periods. However, median ozone concentrations do exhibit the same general trend as CO, with the exception of the mini-monsoon period, which also showed greater vertical structure than the other periods.

[41] Regression of CO and ozone during each period revealed positive correlations in the burning season and mini monsoon, with $R^2 = 0.24$ and 0.28, respectively, and essentially no correlation thereafter, with $R^2 = 0.07$, 0.07 and 0.02 in the premonsoon, active and inactive monsoon periods, respectively. This is consistent with back trajectories over burning sites in the premonsoon phases and a contrasting clean maritime flow in the monsoon phases. There is a return to a positive correlation in the monsoon break ($R^2 = 0.18$) where back trajectories return to a continental origin and hence continental sources. In general, we can conclude that ozone concentrations were low and followed a similar interseasonal trend to CO throughout the campaign.

5.2. Volatile Organic Compounds

[42] Statistical medians, maxima and minima for the nine VOCs detailed in section 2.4 are summarized in Table 6 for each meteorological period. By virtue of their short atmospheric lifetimes and resulting high spatial variability, VOC concentrations are more suited to a case study analysis; however, maxima and minima provided here give an indication of the general interseasonal trend. Concentrations of all VOCs were enhanced in the burning and premonsoon phases as may be expected due to their release by burning vegetation. There was a general decrease in the premonsoon

Table 6. Volatile Organic Carbonaceous Gas Concentration Statistics for Each Meteorological Regime During ACTIVE[a]

	Biomass Burning			Mini-Monsoon			Premonsoon		
Species	Median	Maximum	Minimum	Median	Maximum	Minimum	Median	Maximum	Minimum
ethyl benzene	33	198.6	4.9	20	44.5	3.4	37	388.3	3.7
m + p xylene	85	336.7	12.1	41	106.8	1.7	81	185.8	8.0
o -xylene	36	215.8	6.5	21	54.0	2.1	39	97.5	3.0
nonane	61	264.6	12.4	8	10.2	6.4	96	259.5	31.1
isopropyl benzene	5	45.3	0.2	3	9.4	0.4	7	40.8	1.1
3- ethyltoluene	29	183.2	3.2	16	44.4	0.3	31	61.7	6.3
1,3,5- trimethyl benzene	14	115.3	1.8	8	25.0	0.2	18	35.3	3.6
1,2,4-trimethyl-Benzene	34	172.4	2.5	17	45.7	<LOD	35	77.2	7.0
1,2,3- trimethyl benzene	12	136.7	1.0	9	24.2	<LOD	22	53.0	3.9
propyl benzene	12	87.4	1.8	6	38.6	0.6	13	47.9	2.3
	Active Monsoon			Inactive Monsoon			Monsoon Break		
Species	Median	Maximum	Minimum	Median	Maximum	Minimum	Median	Maximum	Minimum
ethyl benzene	21	65.9	2.0	24	517.7	1.3	14	101.5	0.2
m + p xylene	37	155.9	3.6	45	228.7	1.5	26	154.1	<LOD
o -xylene	20	74.4	3.4	29	299.8	<LOD	13	101.5	0.1
nonane	31	136.3	9.5	38	15.4	<LOD	10	54.2	0.3
isopropyl benzene	4	9.4	0.9	2	52.8	0.2	3	29.3	<LOD
3- ethyltoluene	17	51.7	1.2	4	90.9	0.8	10	38.5	<LOD
1,3,5- trimethyl benzene	7	27.4	0.9	13	103.2	1.0	6	20.3	<LOD
1,2,4-trimethyl-Benzene	12	88.3	0.5	20	252.8	1.8	7	37.7	<LOD
1,2,3- trimethyl benzene	5	17.4	0.7	10	119.5	0.2	2	23.0	<LOD
propyl benzene	5	17.9	0.8	6	53.0	<LOD	3	20.6	<LOD

[a]All concentrations are given in parts per trillion by volume (pptv).

period when this burning stopped, with median concentrations for all species remaining relatively low throughout the monsoon periods and the monsoon break. Maximum concentrations for many species measured in the inactive monsoon phase exceeded those measured even during the burning season, but these represent measurements made in a pollution plume from Darwin measured on a single flight.

5.3. Aerosol Size Distributions

[43] Vertical distributions of total aerosol number concentration derived in the same manner as for CO and ozone are plotted in Figure 5 from the ASP and FSSP, with total number being that integrated over the size ranges 0.3 to 2.5 μm, and 2.5 to 32 μm for the two instruments respectively. The size range integrated for each instrument was based on the 50% transmission of the inlet ($\sim$2.5 μm) in the case of the ASP and the upper size range measurable by the FSSP. As spectra recorded by the ASP measure dry aerosol, and the FSSP samples aerosol at ambient humidity, the ASP spectra were transformed to ambient sizes. This was done using the model described by *Topping et al.* [2005] and

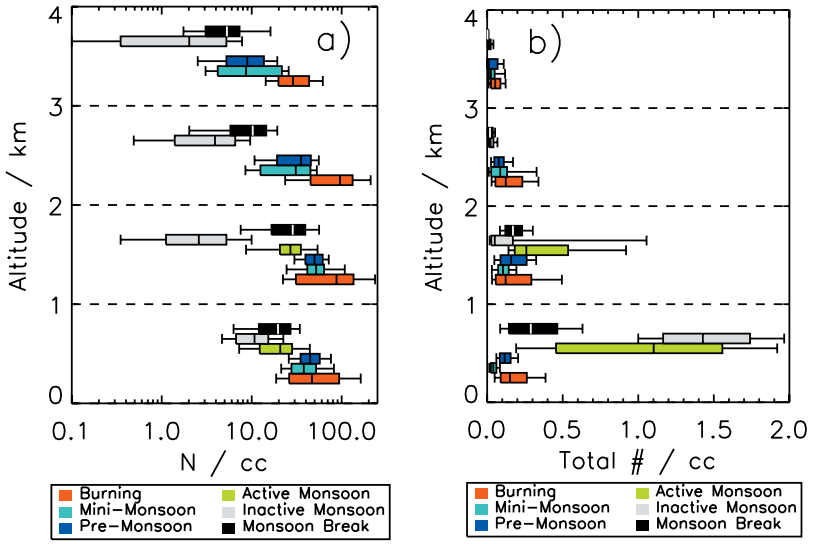

Figure 5. Vertical profiles of aerosol total number concentration calculated (a) from ASP and (b) from FSSP integrated over 0.3 to 2.5 μm; and 2 to 32 μm, respectively. Box center denotes the median; box edges denote the upper and lower quartiles; and extremities denote the 10th and 90th percentiles. Note that measurements were not recorded above 2 km in the active monsoon period.

ambient humidities measured by the AIMMS-20 or Rotronic sensors of the Q-AMS as appropriate (see section 3.1) together with aerosol compositions measured by the Q-AMS. As only total submicron component masses were available, the components were assumed to be internally mixed in the same proportions at all sizes in the accumulation mode. *Topping et al.* [2005] have shown that the approach is capable of accurately predicting the growth factor of mixed component aerosol, and that for mixed inorganic-organic aerosol this growth factor is small. It is of course possible that when significant sea spray aerosols are present, the wet size of the aerosol will be significantly enhanced. This would lead to an underprediction of the ambient size of the aerosol measured by the ASP as sea salt was not measured by the AMS. Growth factors were applied using an exponential fit to the slope of the dry size spectra prior to subsampling each size channel into twenty and resampling the grown population into the original size grid. For the FSSP, data were cloud-cleared using a threshold value of 2 particles per mL integrated over the instrument's size range. Furthermore, owing to the low sensitivity of the FSSP in such a clean environment and hence the poor counting statistics, FSSP data were averaged over a five-minute period to obtain meaningful (nonzero) median concentrations. For both the ASP and FSSP, recorded data were normalized to standard temperature and pressure (20°C, 1001.25 mb) using simultaneously recorded AIMMS-20 data. This pattern of diminishing aerosol number with height is similar to that seen by *Liley et al.* [2002] in the same geographical area and is consistent with dynamics of aerosol source and deposition processes from the surface.

[44] Differences in the pattern of total number between these two instruments throughout the campaign serve to illustrate changes in the fine and coarse aerosol sizes, to which the ASP and FSSP are respectively sensitive. Fine mode aerosols are important when considering scattering of ultraviolet and visible radiation and serve as efficient cloud condensation nuclei (CCN), while the coarse mode contains the majority of the mass and surface area of the aerosol burden, therefore playing an important role in atmospheric chemical processes.

[45] The fine aerosol (ASP; Figure 5a) component varied in the same way as CO throughout the campaign (Figure 4a), with the highest and most variable concentrations measured in the burning period. The high concentrations at that time are explained by the production of smoke from burning vegetation, while the high variability reflects the nature of day-to-day changes in inland fire activity and mixing with cleaner air. There follows a decrease in the fine aerosol concentration and associated variability at the cessation of land clearance, with a continued decrease throughout the premonsoon and monsoon periods, followed by a slight recovery toward a more premonsoon background in the monsoon break. This difference in fine aerosol concentration between the burning phase and the inactive monsoon is in excess of an order of magnitude, with concentrations in the inactive monsoon approaching the limit of instrument sensitivity.

[46] This association between CO and fine mode aerosol is also evident from their positive correlations, which are calculated to be highly significant in the biomass burning and mini-monsoon periods with R^2 values of 0.46 and 0.31, respectively. Such a correlation is essentially absent in the premonsoon, active and inactive monsoon phases with R^2 values of 0.07, 0.05 and 0.02, respectively, before a return to a significant link in the monsoon break ($R^2 = 0.3$). This mirrors the trend (and significance) in correlations calculated between CO and ozone (see section 5.1). Therefore, we can conclude that sources of fine aerosol are closely linked to sources of CO during the biomass burning, mini-monsoon and premonsoon periods, with the dominant source being inland biomass burning during November. The lack of any correlation between fine aerosol and CO concentration in the monsoon phases, coupled with the very small absolute number concentrations of fine aerosol in the active and inactive monsoon periods reflects both the absence of local sources and the efficient removal of these particles in maritime air via precipitation.

[47] The coarse aerosol (FSSP; Figure 5b) component follows this same decreasing trend prior to the monsoon; but in contrast to the fine mode, which is lower in the monsoon periods, we see a large increase in both median number concentration and variability in the monsoon periods compared with the premonsoon and the monsoon break. This change is further illustrated in median size spectra (see Figures 6a, 6b, and 6c). Maxima in the accumulation and coarse modes are observed consistently near 0.3 μm and 10 μm, respectively, although the absence of reliable spectral data below 0.2 μm obscures resolution of the fine mode maximum (see Figure 6c). A consistent peak in one size channel of the FSSP at 8.4 μm is thought to be an instrument artifact. A further potential aerosol mode observed at 0.8 μm is also noted in measurements by the UHSAS instrument and has been noted in previous studies by *Russell-Smith et al.* [2000] of aerosol on the ground in the nearby town of Jabiru using a Grimm spectrometer.

[48] Excellent continuity is seen in the spectra from fine to coarse particle modes measured in the premonsoon periods, but there is a pronounced divergence between spectra measured by the ASP and FSSP in the monsoon phases (the green and grey lines in Figures 6a, 6b and 6c). As a check of the validity of supermicron aerosol data measured by the FSSP, aerosol spectra were compared with a Cloud Aerosol Spectrometer (CAS) onboard the Egrett during its ascent and descent (0.1–3 km) flight phases within their common particle size range. Both instruments compared well, with identical trends and variability observed throughout the campaign.

[49] The AMS could not measure the sea salt component of the aerosol, which would have a much larger growth factor than the sulphate/organic mix which it did measure: 2.91 compared with 1.21 according to the model used here. The discrepancy between FSSP and ASP during the monsoon is consistent with the aerosol having a much higher salt content than in the premonsoon. To test this hypothesis, dry aerosol spectra measured by the ASP were transformed with growth factors appropriate to pure sea salt aerosol. The results are shown in Figures 6d, 6e and 6f, and show a much improved spectral continuity with the measured ambient FSSP spectra. The remaining discrepancy at supermicron sizes can be explained by inlet transmission losses for the ASP, and the likely uncertainty in the measurements (see section 3.2).

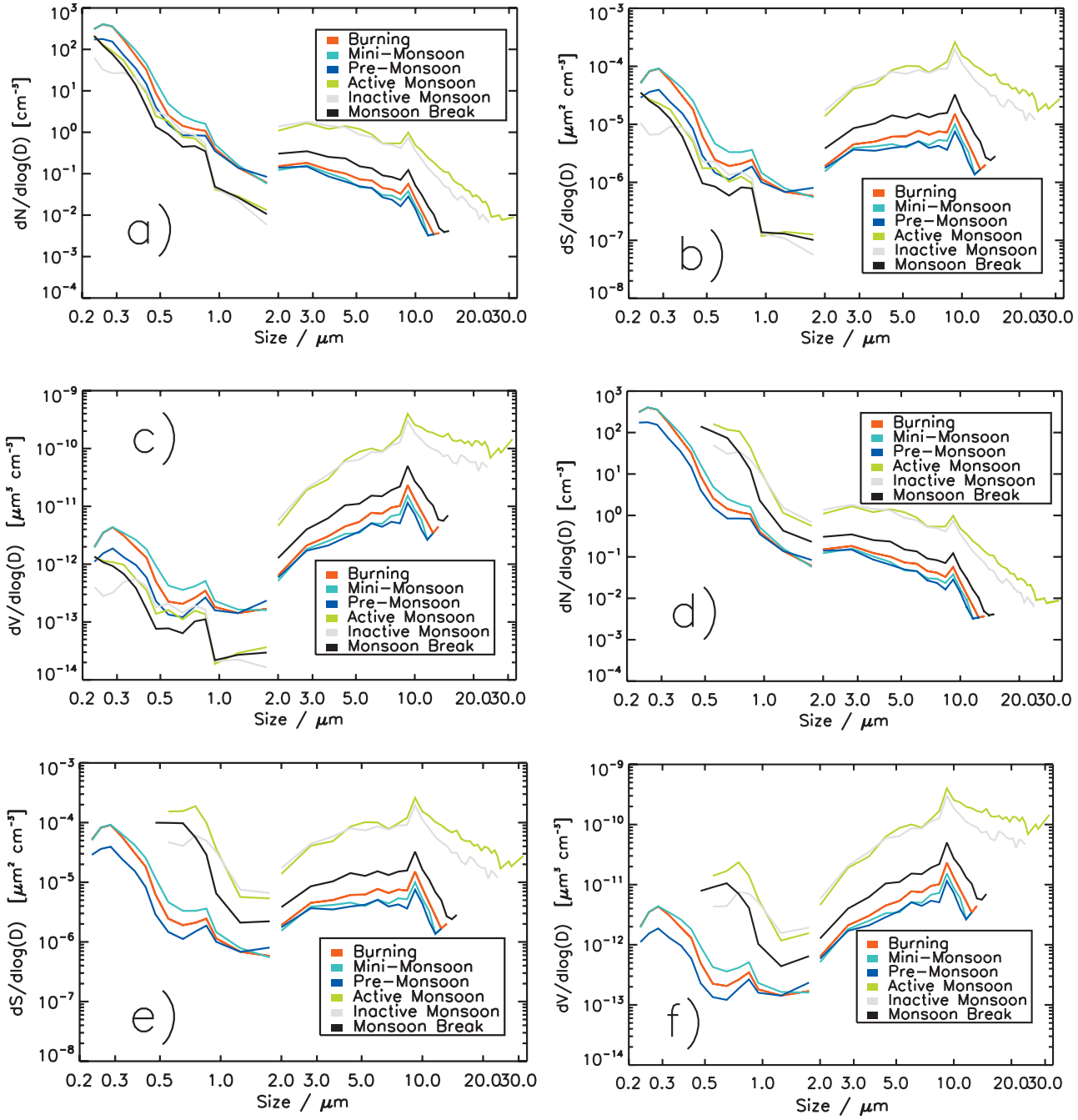

Figure 6. Composite median aerosol size spectra (normalized for size-bin width), color-coded by time period as indicated and measured by the ASP (0.22–1.8 μm) and the FSSP (2.0–32 μm) showing (a) number concentration, (b) surface area, (c) volume, (d) number concentration assuming chloride growth factor, (e) surface area assuming chloride growth factor, and (f) volume assuming chloride growth factor.

[50] During the monsoon periods, back trajectories remained over the ocean for at least five days prior to sampling. Any coarse-mode aerosol from long-range continental sources would be removed by deposition to the ocean over this timescale. Such pure maritime aerosol have been well studied (see review by *O' Dowd et al.* [1997]) with two distinct types identified. These are: (1) primary sea-spray aerosol produced by mechanical disruption of the ocean surface and (2) secondary aerosol in the form of non-sea-salt sulphate and organic species formed by gas-to-particle conversion processes and subsequent cloud processing. Only the former has potential significance in the coarse mode, which is a function of wind speed; with particle size and number concentration typically following an exponential function of wind speed thus: $\log C = aU_{10} + b$, where C is the concentration, U_{10} is the 10 m height wind speed and a and b are constants which depend on particle size. Many such parameterizations have been derived from various

Table 7. Lognormal Fit Parameters and Confidences for Median Aerosol Spectra Within Each Meteorological Period of ACTIVE[a]

	Burning	Mini-Monsoon	Premonsoon	Active Monsoon	Inactive Monsoon	Monsoon Break
			Fine Mode 1			
N_{tot}	203 ± 65	203 ± 57	102 ± 41	272 ± 845	172 ± 619	175 ± 258
$ln(\sigma_g)$	0.23 ± 0.04	0.24 ± 0.04	0.24 ± 0.05	36.6 ± 40.1	0.58 ± 0.48	0.28 ± 0.13
D_g	0.28 ± 0.03	0.29 ± 0.02	0.27 ± 0.03	0.18 ± 0.18	0.13 ± 0.21	0.21 ± 0.09
			Fine Mode 2			
N_{tot}	7.14 ± 14.81	49.7 ± 161.5	5.64 ± 16.02	110 ± 314	0.62 ± 38.3	102 ± 1720
$ln(\sigma_g)$	0.73 ± 0.22	0.81 ± 0.25	0.90 ± 0.43	1.04 ± 2.02	0.78 ± 4.16	1.09 ± 1.27
D_g	0.2 ± 0.3	0.13 ± 0.21	0.21 ± 0.41	0.03 ± 0.53	0.23 ± 6.36	0.03 ± 0.26
			Coarse Mode			
N_{tot}	0.19 ± 0.05	0.14 ± 1.61	0.15 ± 0.04	1.61 ± 0.26	1.61 ± 0.27	0.44 ± 0.14
$ln(\sigma_g)$	0.51 ± 0.06	0.53 ± 0.06	0.54 ± 0.06	0.59 ± 0.03	0.53 ± 0.02	0.54 ± 0.07
D_g	3.61 ± 0.35	3.53 ± 0.38	3.21 ± 0.35	4.40 ± 0.32	4.20 ± 0.26	3.04 ± 0.45

[a]The uncertainty represents the upper and lower 95% confidence level. The fine and coarse mode parameters refer to spectra measured by the ASP and FSSP, respectively.

empirical data [e.g., *Vignati et al.*, 2001; *Gong*, 2003] with a strong dependence on wind speed and humidity.

[51] The spectral shape of the coarse mode fraction in Figure 6d agrees best with that predicted by *Vignati et al.* [2001] at wind speeds in excess of 9 m s^{-1} and high relative humidities (>85%). A full discussion of such parameterizations is beyond the scope of this paper, but we note this agreement here to conclude that the coarse mode fraction measured in the monsoon phases of ACTIVE should predominantly be populated by sea-salt particles. Wind speeds measured by the AIMMS-20 in the marine boundary layer (MBL) during monsoon flights ranged from 4 to 15 m s^{-1} with strong variance within each flight, but generally decreasing throughout the period. Furthermore, relative humidity remained in excess of 85% for much of this time. In noting the strong dependence of sea-salt particle size and production on wind speed, it is postulated that the large spectral variability measured by the FSSP may be explained by the wide range in wind speeds observed in the monsoon period.

5.4. Lognormal Spectral Fits

[52] In order for this aerosol size climatology to be easily used by the reader we have fitted lognormal modes to the data according to the following relationship described further by *Pruppacher and Klett* [1997],

$$\frac{dN}{dD} = \frac{N_{tot}}{D\sqrt{2\pi}\ln\sigma_g}\exp\left(-\frac{\ln^2\left(\frac{D}{D_g}\right)}{2\ln^2\sigma_g}\right), \quad (1)$$

where N_{tot} is the particle number concentration (in particles cm^{-3}), D is the particle diameter (μm), and D_g, σ_g are the number median diameter and the geometric standard deviation of the modal distribution, respectively. For each aerosol size spectrum in each period, two modes were fitted to the fine component and one to the coarse component. The fine and coarse modes were fitted independently. An interactive routine was written to approximately fit the lognormal modes to the size distribution data. These approximate fits were used as an initial guess in a Gauss Newton nonlinear fitting technique to yield the best fit to the data by minimizing the chi-square error on successive iterations. The convergent lognormal parameters and confidences for spectra grown without chloride growth factors applied are given in Table 7. Fine mode spectra with such growth factors applied were fitted best with one mode and are given separately in Table 8.

[53] For the periods without sea salt, the data are well described by the superposition of two lognormal modes; a narrow mode with high concentration in the head of the distribution and a broad mode of typically one hundred times less concentration that extended out to the tail of the distribution. For the monsoon periods and assuming sea-salt composition in the grown spectra, only the broad mode was necessary to achieve the fit.

5.5. Aerosol Composition

[54] Submicron, nonrefractory mass concentrations of four predominant aerosol composition fractions measured by the AMS (sulphate, organics, nitrate and ammonium) are plotted as relative composition by period in Figure 7, together with black carbon (BC) concentrations measured by the PSAP instrument.

[55] First, we note that due to the absence of industrial pollution sources and the generally very clean environment sampled in Darwin, very little ammonium or nitrate was sampled in any period, with vertical profiles generally varying around zero, reflecting random noise caused by ion counting statistics and a high background at the relevant mass-to-charge ratio in the mass spectrum. However, when averaged over many flights, statistically meaningful information could be obtained; even for the worst case of ammonium in the monsoon break, the standard error in the mean was less than 17%.

Table 8. Lognormal Fit Parameters and Confidences for Median Fine-Mode Aerosol Spectra With Pure Chloride Growth Factors Applied for the Monsoon and Monsoon-Break Phases of ACTIVE[a]

	Active Monsoon	Inactive Monsoon	Monsoon Break
N_{tot}	370 ± 1091	45.2 ± 52.0	473 ± 3048
$ln(\sigma_g)$	0.53 ± 0.19	0.45 ± 0.11	0.62 ± 0.40
D_g	0.34 ± 0.37	0.58 ± 0.29	0.21 ± 0.52

[a]Uncertainty represents the upper and lower 95% confidence level.

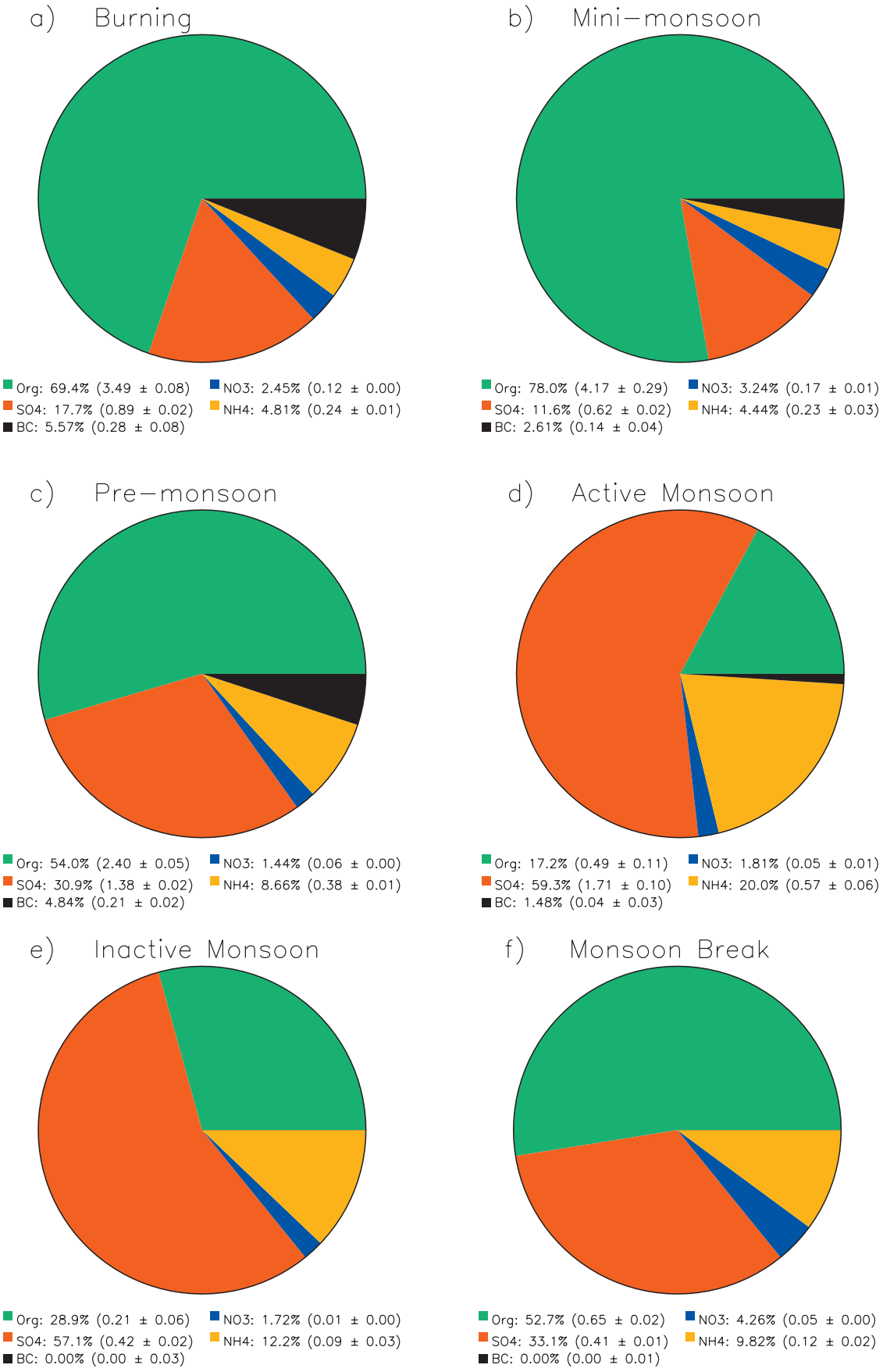
a) Burning
Org: 69.4% (3.49 ± 0.08)
NO3: 2.45% (0.12 ± 0.00)
SO4: 17.7% (0.89 ± 0.02)
NH4: 4.81% (0.24 ± 0.01)
BC: 5.57% (0.28 ± 0.08)
b) Mini−monsoon
Org: 78.0% (4.17 ± 0.29)
NO3: 3.24% (0.17 ± 0.01)
SO4: 11.6% (0.62 ± 0.02)
NH4: 4.44% (0.23 ± 0.03)
BC: 2.61% (0.14 ± 0.04)
c) Pre−monsoon
Org: 54.0% (2.40 ± 0.05)
NO3: 1.44% (0.06 ± 0.00)
SO4: 30.9% (1.38 ± 0.02)
NH4: 8.66% (0.38 ± 0.01)
BC: 4.84% (0.21 ± 0.02)
d) Active Monsoon
Org: 17.2% (0.49 ± 0.11)
NO3: 1.81% (0.05 ± 0.01)
SO4: 59.3% (1.71 ± 0.10)
NH4: 20.0% (0.57 ± 0.06)
BC: 1.48% (0.04 ± 0.03)
e) Inactive Monsoon
Org: 28.9% (0.21 ± 0.06)
NO3: 1.72% (0.01 ± 0.00)
SO4: 57.1% (0.42 ± 0.02)
NH4: 12.2% (0.09 ± 0.03)
BC: 0.00% (0.00 ± 0.03)
f) Monsoon Break
Org: 52.7% (0.65 ± 0.02)
NO3: 4.26% (0.05 ± 0.00)
SO4: 33.1% (0.41 ± 0.01)
NH4: 9.82% (0.12 ± 0.02)
BC: 0.00% (0.00 ± 0.01)

Figure 7

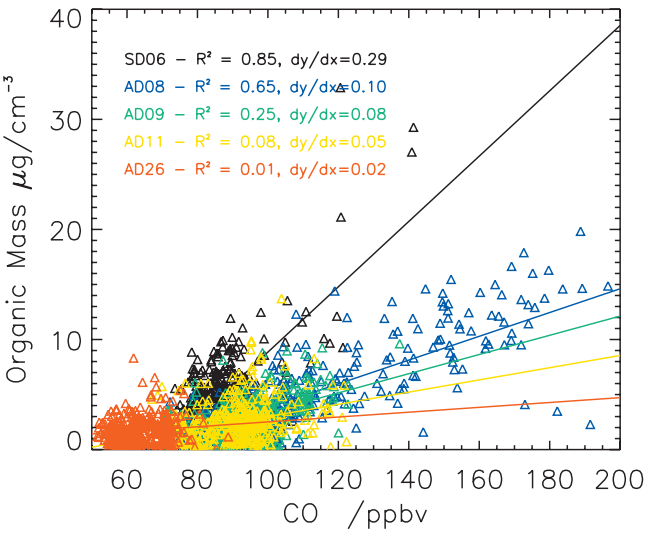

Figure 8. Correlations between measured carbon monoxide and organic aerosol composition over the course of ACTIVE color-coded by flight number as indicated. Periods corresponding to each flight are: SD06, AD08, and AD09 (biomass burning); AD11 (premonsoon); AD26 (monsoon break).

[56] Significant concentrations of sulphate and organic material were sampled in most phases and show contrasting trends which provide useful information for discussions of air mass origin as well as local processes. The variation in organic aerosol loading between the different sampling periods follows the same broad trends as that for CO and fine mode aerosol. However, the correlation between organic mass and CO was strong only during the biomass burning periods. Such correlations are plotted in Figure 8 for a sample of typical flights in the biomass burning, premonsoon and monsoon break periods. No significant correlation was observed in the active or inactive monsoon phases. Each point in Figure 8 represents the simultaneous CO and AMS organic concentration, where CO data are averaged up to 30 s in line with the AMS time response. We see strong correlations ($R^2 = 0.85, 0.65$) between CO and organic aerosol in the early burning phase flights (black and blue in Figure 8), with a clear reduction in dependence throughout the premonsoon and monsoon break phases ($R^2 = 0.25, 0.08$, respectively), illustrating the common burning sources in early flights and the independence of CO from sources of organic aerosol in the later clean phases. The absence of any significant correlation in the active and inactive monsoon phases ($R^2 = 0.01$) is expected in such maritime air masses.

[57] Throughout the burning and premonsoon phases, black carbon concentrations account for roughly 6% of the measured organic mass. Measurements made by *Ward et al.* [1992, 1996] in the regional haze generated by African savanna and Brazilian fires measured around 3% BC in smoldering fires and ~15–20% in active flaming combustion with the exact aerosol makeup being highly dependent on the type of vegetation. However, we see that our measurements of BC in the burning season lie between these two fire regimes suggesting that the air sampled over the Darwin area contained a mix of fire plumes generated in both active and smoldering fires further inland as might be expected. This is comparable with similar measurements of mixed air sampled by *Haywood et al.* [2003] in the SAFARI 2000 experiment, where BC was observed to account for around 5% of the organic mass in burning plumes over Africa. Outside of the burning season, BC concentrations fall rapidly to ~1.5% in the active monsoon phase and falls below the limit of detection (~0.1% by mass) in the inactive monsoon phase and monsoon break.

[58] The evolution in black carbon concentration and its vertical profile throughout the campaign is plotted in Figure 9, noting that PSAP black carbon measurements were not recorded above 1 km during flights in the mini-monsoon phase. Here, we see the same interseasonal evolution at all altitudes as for CO and fine aerosol discussed earlier, with a marked enhancement of soot particles and associated variability in the burning phase (0.4 μg m^{-3}, with extremes of up to 1 μg m^{-3} at the 90th percentile), decreasing by around a factor of two in the premonsoon and dropping to zero in the monsoon phases, albeit at the limit of instrument sensitivity.

[59] Analysis of AMS mass spectra during biomass burning periods offers some insights into the composition of the organic fraction and its transformation in the atmosphere. Figure 10a shows a mass spectrum of organic aerosol close to the source of a large fire. This spectrum is significantly different from that measured near a combustion aerosol source in an urban environment [e.g., *Canagaratna et al.*, 2004] and contains many more oxygenated species and evidence of monoacids such as levoglucosan, identified by unique peaks at m/z 60 and 73 [*Alfarra et al.*, 2007]. Such compounds are known to be directly emitted from biomass burning during the breakdown of lignin [*Jordan et al.*, 2006]. In contrast, a mass spectrum of biomass burning aerosol taken away from the source in the regional haze (Figure 10b) shows a marked change in relative composition with reduced relative abundance of larger mass fragments and a relative increase in m/z 44, representative of a diacid moiety. Similar enhancements have been seen in this fragment in aged continental aerosol in the northern hemisphere [*McFiggans et al.*, 2005]. These different mass spectra reflect a general trend in chemical fractionation of the organic mass as the biomass burning plumes age in the atmosphere.

[60] An example mass spectrum of the organic fraction in clean air (Figure 10c) sampled later in the campaign again shows significant differences from aged continental pollution aerosol [e.g., *Zhang et al.*, 2005] and also from the biomass burning spectra shown in Figures 10a and 10b. The source of this organic aerosol is not clear, but potential origins may include biogenic activity or possibly material from the sea surface microlayer.

Figure 7. Pie charts of relative aerosol composition color-coded as indicated for each time period of ACTIVE. Mass concentrations are quoted as the mean (μg cm^{-3}) over all flights within each period, together with the standard error.

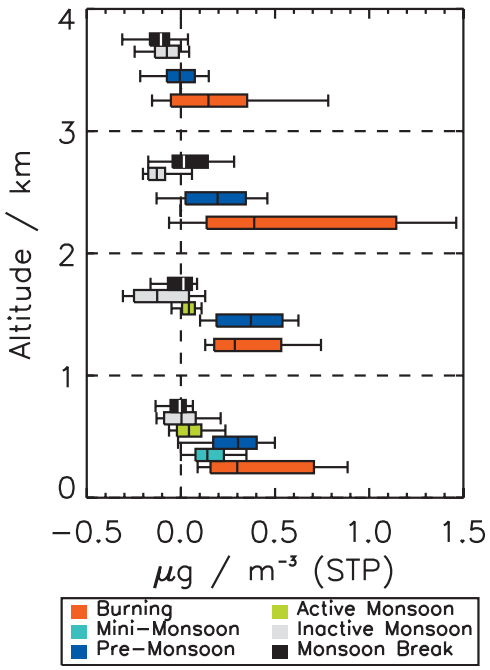

Figure 9. Vertical profile of black carbon (soot) measured by the PSAP, color-coded by time period. Box center denotes the median; box edges denote the upper and lower quartiles; and extremities denote the 10th and 90th percentiles. Note that measurements were not recorded above 2 km in the active monsoon or above 1 km in the mini-monsoon period.

[61] The organic mass fractions in both the biomass burning and clean periods are chemically distinctly different to those previously seen in anthropogenic-dominated midlatitude environments [e.g., *Zhang et al.*, 2005]. The sources, chemical nature and potential atmospheric implications of these organic aerosols will be discussed in future publications.

[62] In contrast to the enhancement of the organic fraction, sulphate composition is only marginally higher in the burning season than the premonsoon, with a marked increase in terms of both median mass and associated variability in the active monsoon phase. This dramatic change in sulphate variability in the active monsoon follows trends (of increased concentrations) observed in the coarse aerosol mode (recall Figure 5b). It is highly likely that this enhanced sulphate is the result of oxidation of SO_2 by peroxide in solution, which can take place rapidly in cloud droplets near cloud base [*Ayers and Larson*, 1991; *Hegg*, 1992]. Should the pH rise sufficiently on droplet activation (become more neutral), S(IV) oxidation rates may be enhanced by ozone, as was observed by *Lowe et al.* [1995] when cloud droplets were nucleated on relatively pH-neutral sea-salt aerosol. In summary, we deduce that enhanced submicron sulphate aerosol observed in the maritime monsoon air results from oxidative processing of SO_2 in cloud droplets. As was observed during ACE-1 [*Mari et al.*, 1998] di-methyl sulphide is the main source of sulphur in very clean, remote marine environments.

[63] Interestingly, sulphate was much reduced and much less variable in the inactive monsoon, while coarse mode aerosol continued at high concentrations. Given the measurements available it is not possible to comment further on the exact mechanism leading to this observation as there are many possible reasons for reduced sulphate aerosol, such as reduced DMS emission, wet deposition further upwind, or a reduction in local cloud cover (and hence cloud processing) in the inactive monsoon. However, despite the reduction in overall loadings, the ratio of sulphate to ammonium was high in the inactive monsoon phase indicating that aerosols were more acidic than in other periods of the campaign; the ratio of sulphate mass to ammonium mass in those periods approached the molar ratio limit for molecular ammonium sulphate of 2.67, indicating that aerosols were generally pH neutral.

[64] The nitrate fraction remained relatively small at around 1–4% of the total mass fraction considered here and is arguably smaller in the monsoon phases as might be expected by its nature as a marker of continental pollution. However, such low signals within the AMS mass spectra, it is difficult to confidently state that the reported nitrate originates from ammonium nitrate, as is usual during continental sampling. Other species may be responsible for small amounts of reported nitrate, such as mineral or organic nitrates, or amines [*Allan et al.*, 2004b].

6. Conclusions

[65] This paper describes the first measurements of gas phase species and aerosol size and composition in the tropical planetary boundary layer near Darwin, Australia as measured onboard aircraft operated as part of the ACTIVE campaign between November 2005 and February 2006.

[66] Six periods of contrasting conditions in the background environment were identified during the campaign, which include a dry period of significant local, and more remote, land-clearance burning, followed by an intermediate period with no burning prior to a wet and subsequently dry monsoon phase and a later monsoon break. Of these, all periods except for the monsoon phases were characterized by daily isolated deep convective storms over the Darwin area and the nearby Tiwi Islands, capable of rapidly transporting boundary layer air to the TTL.

[67] Carbon monoxide, fine mode aerosol, black carbon and organic aerosol loading all follow the same broad trends when comparing the different air mass periods. This mostly reflects influences from biomass burning with both fresh and secondary organic aerosols identified during the active burning phase. All were greatly reduced in the monsoon phases which carried maritime air into the Darwin area. Ozone was highly variable but very low compared to northern hemispheric backgrounds at all times and broadly followed a similar evolution to CO and organic loadings. During the biomass burning period CO, aerosol fine mode number concentration and organic mass were positively and significantly correlated.

[68] Coarse-mode (supermicron) number concentration and fine-mode (submicron) sulphate aerosol loading were greatly enhanced in the active monsoon period indicating potentially significant sulphate aerosol production via aque-

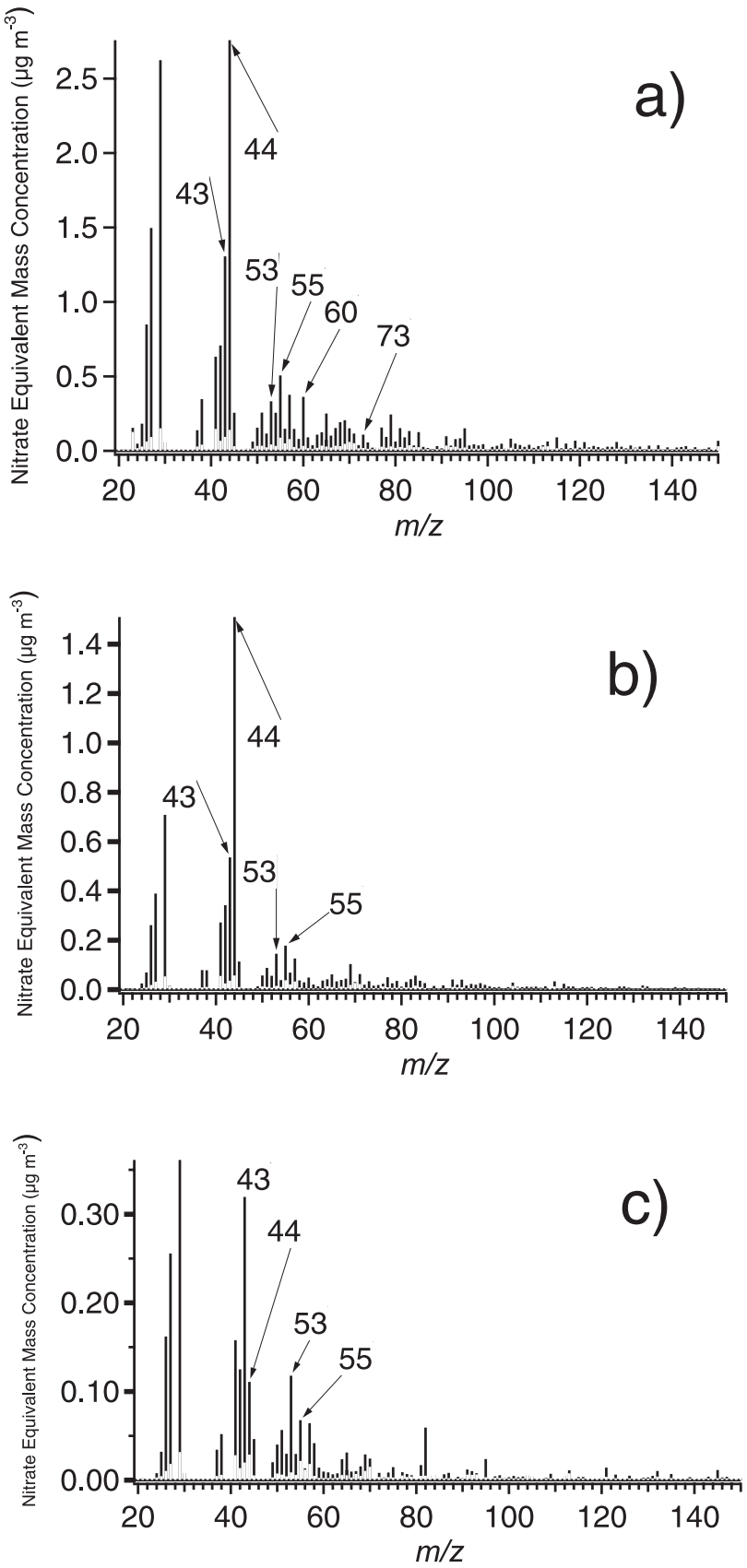

Figure 10. Typical mass spectra recorded by the AMS normalized to nitrate equivalent mass concentration for flight: (a) SD05, a flight in the plume of an active inland scrub fire in the mini-monsoon period; (b) AD04, a flight through haze layer in the biomass burning period; and (c) AD25, a clean flight in the monsoon break.

ous phase S(IV) oxidation in cloud droplets activated on sea-salt aerosol lofted by mechanical disturbance of the ocean surface by high winds associated with the monsoon. Measured coarse mode spectra in the monsoon appear to agree well with the parameterization by *Vignati et al.* [2001] for sea-salt production in the range of wind speeds measured at this time. The sulphate aerosol component was reduced in the dry monsoon, possibly due to a reduction in cloud presence and hence cloud processes leading to sulphate production. However, high winds may have continued to loft large sea-salt particles, accounting in part for the large number of coarse mode aerosol at that time.

[69] Nitrate and ammonium loadings were observed to be small and close to the limit of instrument sensitivity, although ammonium concentrations relative to sulphate after averaging indicates mostly pH-neutral aerosol for all but the monsoon phases where it may have been more acidic.

[70] This data set provides a reference of background conditions in the boundary layer across a wide range of meteorological and local conditions encountered in the Darwin region and offers valuable new information relating to the inflow to deep tropical convective storms in the area and over the nearby Tiwi Islands. Modeling studies currently in progress are using the aerosol results reported here to calculate cloud condensation nuclei concentrations. Together with the gas phase measurements, these are used as input to models of deep convection which predict the composition of air lifted from the boundary layer to the TTL.

[71] **Acknowledgments.** We thank NERC for funding the ACTIVE project and the NERC Airborne Research and Survey Facility (ARSF) for operational support of the Dornier-228 aircraft. This project would not have been possible without the extensive support of the Australian Bureau of Meteorology, in particular Peter May at the Bureau of Meteorology Research Centre, Melbourne, and Lori Chappel at the Regional Forecasting Centre in Darwin. We also thank the RAAF base, Darwin, for hosting the aircraft and campaign base, and for their logistical support.

References

Agarwal, J. K., and G. J. Sem (1980), Continuous flow single-particle-counting condensation nuclei counter, *J. Aerosol Sci.*, *11*, 343–357.

Alfarra, M. R., et al. (2007), Identification of the mass spectral signature of organic aerosols from wood burning emissions, *Environ. Sci. Technol.*, *41*(16), 5770–5777.

Allan, J. D., J. L. Jimenez, P. I. Williams, M. E. Alfarra, K. N. Bower, J. T. Jayne, H. Coe, and D. R. Worsnop (2003), Quantitative sampling using an Aerodyne mass spectrometer: 1. Techniques of data interpretation and error analysis, *J. Geophys. Res.*, *108*(D3), 4090, doi:10.1029/2002JD002358.

Allan, J. D., et al. (2004a), A generalised method for the extraction of chemically resolved mass spectra from Aerodyne aerosol mass spectrometer data, *J. Aerosol. Sci.*, *35*, 909–922.

Allan, J. D., et al. (2004b), Submicron aerosol composition at Trinidad Head, California, during ITCT 2K2: Its relationship with gas phase volatile organic carbon and assessment of instrument performance, *J. Geophys. Res.*, *109*, D23S24, doi:10.1029/2003JD004208.

Ayers, G. P., and T. V. Larson (1991), Numerical study of droplet size dependent chemistry in oceanic wintertime stratus cloud at southern mid-latitudes, *J. Atmos. Chem.*, *11*, 143–167.

Baron, P. A., and K. Willeke (Eds.) (1993), *Aerosol Measurement: Principles, Techniques, and Applications*, pp. 179–180, Van Nostrand Reinhold, New York.

Baumgardner, D., W. Strapp, and J. E. Dye (1985), Evaluation of the forward Scattering Spectrometer Probe – Part II: Corrections for coincidence and dead-time losses, *J. Atmos. Oceanic Technol.*, *2*, 626–632.

Beswick, K. M., M. W. Gallagher, A. R. Webb, E. G. Norton, and F. Perry (2007), Application of the Aventech AIMMS20AQ airborne probe for turbulence measurements during the Convective Storm Initiation Project, *Atmos. Chem. Phys. Discuss.*, *7*, 3519–3555.

Canagaratna, M. R., et al. (2004), Chase studies of particulate emissions from in-use New York City vehicles, *Aerosol Sci. Technol.*, *38*, 555–573.

Carr, S. B., J. L. Gras, M. T. Hackett, and M. D. Keywood (2005), Aerosol characterisation in the Northern Territory of Australia during the dry season with an emphasis on biomass burning, *DSTO-RR-0298*, Defence Sci. and Technol. Org., Melbourne, Victoria, Australia.

Crook, N. A. (2000), Understanding Hector: The dynamics of island thunderstorms, *Mon. Weather Rev.*, *129*(6), 1550–1563.

Crosier, J., J. D. Allan, H. Coe, K. N. Bower, P. Formenti, and P. I. Williams (2006), Chemical composition of summertime aerosol in the Po Valley (Italy), Northern Adriatic and Black Sea, Submitted to *Q. J. R. Meteorol. Soc.*, *133*, 61–75.

Cross, E. S., J. G. Slowik, P. Davidovits, J. D. Allan, D. R. Worsnop, J. T. Jayne, D. K. Lewis, M. Canagaratna, and T. B. Onasch (2007), Laboratory and ambient particle density determinations using light scattering in conjunction with aerosol mass spectrometry, *Aerosol Sci. Technol.*, *41*, 343–359.

Davies, D., S. Kumar, and J. Descloitres (2004), Global fire monitoring using MODIS near-real-time satellite data, *GIM Int.*, *18*(4), 41–43.

Dessler, A. E. (2002), The effect of deep tropical convection on the tropical tropopause layer, *J. Geophys. Res.*, *107*(D3), 4033, doi:10.1029/2001JD000511.

Edwards, D. P., et al. (2006), Satellite-observed pollution from Southern Hemisphere biomass burning, *J. Geophys. Res.*, *111*, D14312, doi:10.1029/2005JD006655.

Esler, J. G., D. G. H. Tan, P. H. Haynes, M. J. Evans, K. S. Law, P. Plantevin, and J. A. Pyle (2001), Stratosphere-troposphere exchange: Chemical sensitivity to mixing, *J. Geophys. Res.*, *106*(D5), 4717–4732.

Fiebig, M. (2001), The tropospheric aerosol at midlatitudes—Microphysics, optics, and climate forcing illustrated by the LACE 98 study, *DLR-Forsch. 2001-23*, German Aerospace Cent., Cologne, Germany.

Giglio, L., J. Descloitres, C. O. Justice, and Y. J. Kaufman (2003), An enhanced contextual fire detection algorithm for MODIS, *Remote Sens. Environ.*, *87*, 273–282.

Gloudemans, A. M. S., M. C. Krol, J. F. Meirink, A. T. J. de Laat, G. R. van der Werf, H. Schrijver, M. M. P. van den Broek, and I. Aben (2006), Evidence for long-range transport of carbon monoxide in the Southern Hemisphere from SCIAMACHY observations, *Geophys. Res. Lett.*, *33*, L16807, doi:10.1029/2006GL026804.

Gong, S. L. (2003), A parameterisation of sea-salt aerosol source function for sub- and super-micron particles, *Global Biogeochem. Cycles*, *17*(4), 1097, doi:10.1029/2003GB002079.

Haywood, J. M., S. R. Osborne, P. N. Francis, A. Keil, P. Formenti, M. O. Andreae, and P. H. Kaye (2003), The mean physical and optical properties of regional haze dominated by biomass burning aerosol measured from the C-130 aircraft during SAFARI 2000, *J. Geophys. Res.*, *108*(D13), 8473, doi:10.1029/2002JD002226.

Hegg, D. A. (1992), Modeling the effects of heterogeneous cloud chemistry on the marine particle size distribution, *J Geophys. Res.*, *97*(D12), 12,927–12,933.

Heintzenberg, J., D. C. Covert, and R. van Dingenen (2000), Size distribution and chemical composition of marine aerosols: A compilation and review, *Tellus, Ser. B*, *52*(4), 1104–1122.

Intergovernmental Panel on Climate Change (2001), *Climate Change 2001: The Scientific Basis. Contribution of Working Group I to the Third Assessment Report of the Intergovernmental Panel on Climate Change*, edited by J. T. Houghton et al., 881 pp., Cambridge Univ. Press, Cambridge, U.K.

Jayne, J. T., D. C. Leard, X. F. Zhang, P. Davidovits, K. A. Smith, C. E. Kolb, and D. R. Worsnop (2000), Development of an aerosol mass spectrometer for size and composition analysis of submicron particles, *Aerosol Sci. Technol.*, *33*, 49–70.

Jimenez, J. L., et al. (2003), Ambient aerosol sampling using the Aerodyne Aerosol Mass Spectrometer, *J. Geophys. Res.*, *108*(D7), 8425, doi:10.1029/2001JD001213.

Jordan, T. B., A. J. Seen, and G. E. Jacobsen (2006), Levoglucosan as an atmospheric tracer for woodsmoke, *Atmos. Environ.*, *40*, 5316–5321.

Kondo, Y., M. Ko, M. Koike, S. Kawakami, and T. Ogawa (2002), Preface to special section on Biomass Burning and Lightning Experiment (BIBLE), *J. Geophys. Res.*, *107*, 8397, doi:10.1029/2002JD002401, [printed *108*(D3), 2003].

Lefohn, A. S., S. J. Oltmans, T. Dann, and H. B. Singh (2001), Present-day variability of background ozone in the lower troposphere, *J. Geophys. Res.*, *106*(D9), 9945–9958.

Liley, J. B., et al. (2002), Black carbon in aerosol during BIBLE B, *J. Geophys. Res.*, *107*, 8399, doi:10.1029/2001JD000845, [printed *108*(D3), 2003].

Liu, Y., and P. H. Daum (2000), The effect of refractive index on size distributions and light scattering coefficients derived from optical particle counters, *J. Aerosol Sci.*, *31*, 945–957.

Lohmann, U., and J. Feichter (2005), Global indirect aerosol effects: A review, *Atmos. Chem. Phys.*, *5*, 715–737.

Lowe, J. A., M. H. Smith, S. L. Clegg, and C. D. O'Dowd (1995), Influence of sub-micron sea-salt aerosols on sulphate production in marine clouds, *Rep. GR9/1020*, Nat. Environ. Res. Counc., Swindon, U.K.

Manton, M. J., and J. L. McBride (1992), Recent research on the Australian Monsoon, *J. Meteorol. Soc. Jpn.*, *70*, 275–285.

Mari, C., K. Suhre, T. S. Bates, J. E. Johnson, R. Rosset, A. R. Bandy, F. L. Eisele, R. L. Mauldin, and D. C. Thornton (1998), Physico-chemical modeling of the first aerosol Characterization Experiment (ACE 1) Lagrangian B: 2. DMS emission, transport, and oxidation at the mesoscale, *J. Geophys. Res.*, *103*(D13), 16,457–16,473.

McFiggans, G., et al. (2005), Simplification of the representation of the organic component of atmospheric particulates, *Faraday Discuss.*, *130*, 341–362.

McFiggans, G., et al. (2006), The effect of physical and chemical aerosol properties on warm cloud droplet activation, *Atmos. Chem. Phys.*, *6*, 2593–2649.

O'Dowd, C. D., M. H. Smith, I. E. Consterdine, and J. A. Lowe (1997), Marine aerosol, seal-salt, and the marine sulphur cycle: A review, *Atmos. Environ.*, *31*, 73–80.

Petzold, A., M. Fiebig, H. Flentje, A. Keil, U. Leiterer, F. Schröder, A. Stifter, M. Wendisch, and P. Wendling (2002), Vertical variability of aerosol properties observed at a continental site during the Lindenberg Aerosol Characterization Experiment (LACE 98), *J. Geophys. Res.*, *107*(D21), 8128, doi:10.1029/2001JD001043.

Pruppacher, H. P., and J. D. Klett (Eds.) (1997), *Microphysics of Clouds and Precipitation*, 26 pp., Kluwer Acad., Norwell, Mass.

Robinson, A. D., J. D. McIntyre, N. R. P. Harris, J. A. Pyle, P. G. Simmonds, and F. Danis (2000), A lightweight balloon-borne gas chromatograph for in situ measurements of atmospheric halocarbons, *Rev. Sci. Instrum.*, *71*(12), 4553–4560.

Russell-Smith, J., G. Allan, R. Thackway, T. Rosling, and R. Smith (2000), Fire Management and Savannah Landscapes in Northern Australia, in *Fire and Sustainable Agricultural and Forestry Development in Eastern Indonesia and Northern Australia, ACIAR Proc.*, vol. 91, pp. 05–101, Aust. Cent. for Int. Agric. Res., Canberra, ACT, Australia.

Russell-Smith, J., C. Edwards, and G. D. Cook (2003), Reliability of biomass burning estimates from savanna fires: Biomass burning in northern Australia during the 1999 Biomass Burning and Lightning Experiment B field campaign, *J. Geophys. Res.*, *108*(D3), 8405, doi:10.1029/2001JD000787.

Saxton, J. E., A. C. Lewis, J. H. Kettlewell, M. Z. Ozel, F. Gogus, Y. Boni, S. O. U. Korogone, and D. Serça (2007), Isoprene and monoterpene emissions from secondary forest in northern Benin, *Atmos. Chem. Phys. Discuss.*, *7*, 4981–5012.

Staudt, A. C., D. J. Jacob, J. Logan, D. Bachiochi, T. N. Krishnamurti, and G. W. Sachse (2001), Continental sources, transoceanic transport, and interhemispheric exchange of carbon monoxide over the Pacific, *J. Geophys. Res.*, *106*(D23), 32,571–32,590.

Stohl, A., et al. (2003), Stratosphere-troposphere exchange: A review, and what we have learned from STACCATO, *J. Geophys. Res.*, *108*(D12), 8516, doi:10.1029/2002JD002490.

Takegawa, N., Y. Miyazaki, Y. Kondo, Y. Komazaki, T. Miyakawa, J. L. Jimenez, J. T. Jayne, D. R. Worsnop, J. D. Allan, and R. J. Weber (2005), Characterization of an Aerodyne Aerosol Mass Spectrometer (AMS): Intercomparison with other aerosol instruments, *Aerosol Sci. Technol.*, *39*, 760–770.

Topping, D. O., G. B. McFiggans, and H. Coe (2005), A curved multi-component aerosol hygroscopicity model framework: 2. Including organics, *Atmos. Chem. Phys.*, *5*, 1223–1242.

Vaughan, G., C. Schiller, A. R. MacKenzie, K. N. Bower, T. Peter, H. Schlager, N. R. P. Harris, and P. T. May (2008), Studies in a natural laboratory: High-altitude aircraft measurements around deep tropical convection, *Bull. Am. Meteorol. Soc*, in press.

Vignati, E., G. de Leeuw, and R. Berkowicz (2001), Modeling coastal aerosol transport and effects of surf-produced aerosols on processes in the marine atmospheric boundary layer, *J. Geophys. Res.*, *106*(D17), 20,225–20,238.

Ward, D. E., R. A. Susott, J. B. Kaufman, R. E. Babbitt, D. L. Cummings, B. Dias, B. N. Holben, Y. J. Kaufman, R. A. Rasmussen, and A. W. Setzer (1992), Smoke and fire characteristics for cerrado and deforestation burns in Brazil: Base-B experiment, *J. Geophys. Res.*, *97*(D13), 14,601–14,619.

Ward, D. E., W. M. Hao, R. A. Susott, R. E. Babbitt, R. W. Shea, J. B. Kaufman, and C. O. Justice (1996), Effect of fuel composition on combustion efficiency and emission factors for African savanna ecosystems, *J. Geophys. Res.*, *101*(D19), 23,569–23,576.

Zhang, Q., M. R. Alfarra, D. R. Worsnop, J. D. Allan, H. Coe, M. R. Canagaratna, and J. L. Jimenez (2005), Deconvolution and quantification of hydrocarbon-like and oxygenated organic aerosols based on aerosol mass spectrometry, *Environ. Sci. Technol.*, *39*, 4938–4952.

J. Allan, G. Allen, K. N. Bower, T. W. Choularton, H. Coe, P. Connolly, J. Crosier, M. Flynn, M. Gallagher, G. Vaughan, and P. I. Williams, Centre for Atmospheric Science, University of Manchester, Sackville Street Building, Sackville Street, Manchester M60 1QD, UK. (grant.allen@manchester.ac.uk)

J. F. Hamilton, J. D. Lee, A. C. Lewis, J. E. Saxton, and N. M. Watson, Department of Chemistry, University of York, Heslington, York YO10 5DD, UK.